Interaction Notes

Note 460

6 Nov 1987

Monitoring and Quantifying Electromagnetic Penetration Through Apertures

F. C. Yang
C. Zuffada
Dikewood Division of Kaman Sciences Corporation
Santa Monica, California 90405

Abstract

Techniques to monitor and quantify the shielding performances of hardening fixes for windows and doors of aircraft are presented for the frequency range of 0-200 MHz. This frequency range includes resonance frequencies of some larger doors. A characterization of the drivers to be used for monitoring tests is also described. Comparisons between the quantification predictions and some experimental results are reported.

PREFACE

The authors wish to thank W. D. Prather, T. Smith, C. E. Baum, and C. D. Taylor of AFWL, and K.S.H. Lee of Kaman/Dikewood for their support and suggestions.

TABLE OF CONTENTS

1.0 INTRODUCTION

The hardening against electromagnetic (EM) penetration through apertures can be provided by such elements as screens and gaskets which, once installed, become permanent parts of the airframe. These EM hardening fixes may degrade with time, thus making the onboard periodic monitoring a necessity. In this note, we suggest several approaches to monitor the shielding performance of these hardening fixes for window and door apertures whose sizes range from being electrically small to dimensions comparable to wavelengths. The note starts with a description of monitoring approaches and simple analysis to quantify the penetration through hardened/unhardened apertures (Sections II and III). In each approach, an appropriate driver is suggested for generating electromagnetic fields. The driver selected for monitoring will be either a parallel-plate or a two-wire (rhombic) simulator. By properly choosing the parameters of the driver, highly uniform fields over the area covering the aperture can be obtained, as will be described in Section IV. Recently, measurements of EMP penetration onboard a testbed aircraft have been taken in the frequency range of 0-200 MHz [Ref. 1]. A comparison between the test and analytical results is made in Section V. Finally, a brief summary and some concluding remarks are given in Section VI.

2.0 MONITORING AND QUANTIFYING PENETRATION THROUGH ELECTRICALLY SMALL APERTURES

An aperture is considered to be electrically small if its perimeter (p) is small compared to the wavelength (λ) of the driving field (say, $p < \lambda/8$). For the frequency (f) range of interest from DC to 200 MHz, this is generally true for windows of most aircraft but is no longer true for most doors except in the low end of the frequency band (say, $f \lesssim 10$ MHz). The monitoring techniques and the analytical approximations given in this section are thus intended for windows up to 200 MHz and doors up to about 10 MHz. More general techniques and analytical approximations applicable for electrically larger doors will be discussed in the next section.

The electromagnetic penetration through an electrically small aperture can be decoupled into the electric and magnetic field penetrations [Ref. 2]. The following is a discussion of several techniques to monitor these penetrations. The discussion will divide the apertures into two categories, namely, simple apertures such as windows and open doors, and hatch apertures such as closed doors with slits.

2.1 Penetration Through Simple Apertures

The quantities to characterize the penetration are the maximum magnetic flux Φ for magnetic penetration and the total electric flux Q for electric penetration. When the aperture is not hardened, these fluxes are [Refs. 3,4,5]

$$\Phi \simeq H_{sc}\mu_o \ell^2/4 \qquad (1)$$

$$Q \simeq E_{sc}\varepsilon_o A/2 \qquad (2)$$

where ℓ is the effective diameter of the aperture, A is the area of the aperture, μ_o is the free-space permeability, ε_o is the free-space permittivity, and H_{sc} and E_{sc} are, respectively, the short-circuit magnetic and electric fields. Equation 1 is applicable for an aperture with low eccentricity (i.e., length $\simeq$ width $\simeq \ell$) and is derived from the field distribution at a circular aperture given in Ref. 4, while Equation 2 is directly quoted from Ref. 5.

When the aperture is hardened by either wire meshes or conductive coating, these fluxes are reduced by the factor [Refs. 2, 3]

$$f_h = (1 + sL_a/Z_h)^{-1} \qquad \text{(for magnetic penetration)} \qquad (3)$$

$$f_e = (1 + (sC_aZ_e)^{-1})^{-1} \qquad \text{(for electric penetration)} \qquad (4)$$

where

$$L_a \simeq 2\mu_o A/p, \quad C_a \simeq 8\varepsilon_o A/p$$

$$Z_h \simeq \begin{cases} Z'_w a_s + \dfrac{s\mu_o a_s}{2\pi} \ell n \left(\dfrac{a_s}{2\pi r_w}\right) & \text{(wire mesh)} \\ (\sigma\Lambda)^{-1} & \text{(conductive coating)} \end{cases}$$

$$Z_e \simeq \begin{cases} (sC_e)^{-1} = 3\pi/(4sC_a\beta_e) & \text{(wire mesh)} \\ (\sigma\Lambda)^{-1} & \text{(conductive coating)} \end{cases}$$

and

$$Z'_w = (\pi r_w^2 \sigma_w)^{-1}$$

$$\beta_e = \frac{3\pi}{4}\frac{C_e}{C_a} \simeq \frac{p\varepsilon_r}{2}\left[a_s \ell n \left(\frac{a_s}{2\pi r_w}\right)\right]^{-1}$$

a_s, r_w, ε_r, σ_w = separation, radius, dielectric constant, conductivity of the wire meshes

σ, Λ = conductivity and thickness of the conductive coating

$s = j\omega = j2\pi f$

To monitor the electric penetration through such an aperture, one can use a monitoring wire/bowl to collect the penetrant electric flux (Ref. 6, Fig. 1a).

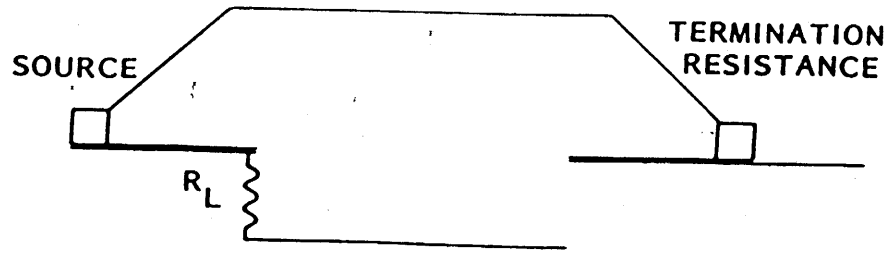

(a)

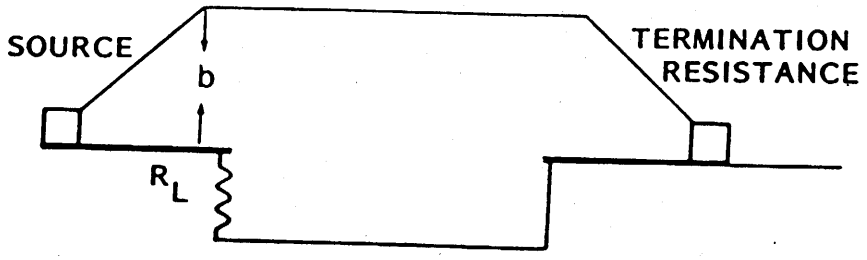

(b)

Figure 1. Monitoring approaches to measure electric or magnetic penetration.
a. side view - electric penetration.
b. side view - magnetic penetration.

The signal picked up by the monitoring wire/bowl can be estimated by using the circuit described in Fig. 2 where C_b is the capacitance of the monitoring wire/bowl with respect to its surrounding. In the circuit, one can set $R_L = 0$ and then use a current probe to measure the current through the load, in which case one has

$$I_p = sQ\, f_e f_\ell \tag{5}$$

where f_ℓ is a function of the location of the monitoring wire/bowl introduced to account for the reduction in the measured flux when it is unable to collect all the penetrant electric flux.

If the current probe has a transfer impedance equal to R Ω, then the recorded voltage is

$$V_p = RI_p = sQR\, f_e f_\ell \tag{6}$$

One can also take $R_L = 50\ \Omega$ and measure the voltage across the resistor, which is given by

$$V_R \simeq sQ \frac{R_L}{1 + sC_b R_L} f_e f_\ell \tag{7}$$

Since C_b is about 10^{-11}F, with $R_L = 50\ \Omega$ and for frequencies below 200 MHz one has

$$V_R \simeq sQR_L\, f_e f_\ell \tag{8}$$

For $R_L > R$ monitoring with R_L gives higher sensitivity.

Since the measuring technique is intended for monitoring the shielding performance of a hardening fix during its life cycle, one would maintain the same driver and monitoring arrangement. That is to say, to keep Q and f_ℓ approximately unchanged. Under such a condition, a change in V_p (or V_R) will be a direct indication of change in shielding performance.

To monitor the magnetic penetration, similar techniques may be used. The monitoring wire can be either next to the window or receded from the window. When the monitoring wire is next to the window it has the maximum flux linkage, whereas the linking flux is reduced if the wire is moved away. The

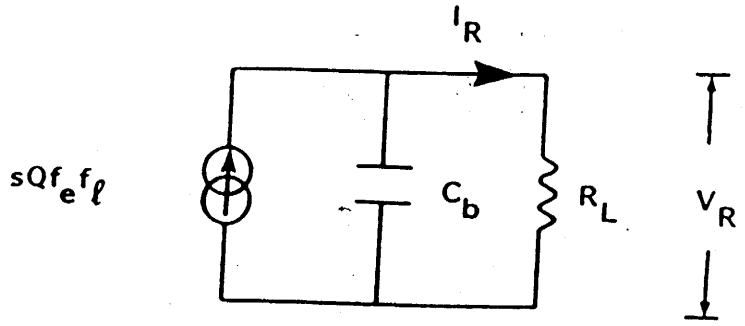

Figure 2. Circuit representation of monitoring scheme for electric penetration.

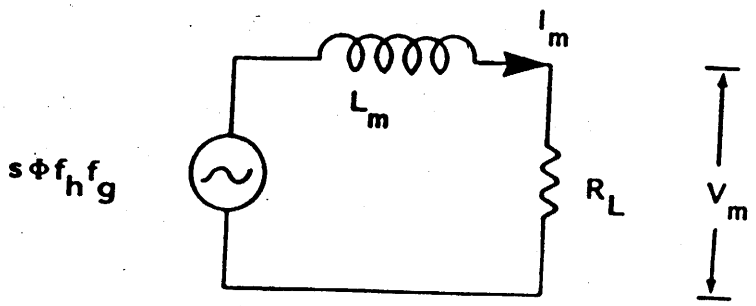

Figure 3. Circuit representation of monitoring scheme for magnetic penetration.

equivalent circuits shown in Fig. 3 can be used to relate the measured responses to the penetrant flux. Here L_m is the inductance of the monitoring wire and f_g (similar to f_ℓ for electric field penetration) is a geometrical factor to quantify the reduction when the monitoring wire is receded from the window. From Fig. 3, one has for the measured current

$$I_m \simeq s\Phi\, f_h f_g/(sL_m + R_L)$$

Since the precise value of L_m is difficult to obtain, one would use a load resistance such that $R_L >> |sL_m|$. Thus

$$I_m \simeq s\Phi\, f_h f_g/R_L$$

which can be monitored by a current probe. For a typical window, to maintain $R_L >> |sL_m|$ up to 200 MHz, the required R_L could be larger than 1 kΩ. Such a high resistance may reduce the measured quantity to a level of very low signal-to-noise ratio. Since this technique is primarily intended for monitoring the shielding performance of a hardening fix during its life cycle, the knowledge of the absolute value of f_h is not necessary. The important quantity is how f_h varies from a baseline value obtained when the hardening fix met its specified requirement. Thus, it is suggested that a R_L = 50 Ω be used as an alternative. This can be accomplished by soldering one end of the monitoring wire to the center conductor of a 50 Ω coaxial cable which is grounded to the airframe and connected to the monitoring instrument. This arrangement will have less problem concerning low signal-to-noise ratio. If the monitoring driver and wire are kept unchanged, the shielding performance variation is simply the change in the measured current I_m, which is equal to $V_m/50$, V_m being the measured voltage.

2.2 Penetration Through Hatch Apertures

The quantities to characterize the penetration through a hatch aperture are again Φ for the magnetic penetration and Q for the electric penetration. To simplify the discussion, only rectangular hatch apertures will be considered. Hatch apertures of other shapes can be approximated by rectangular ones.

Even for unhardened hatch apertures, two different situations need be

considered. A door is always connected to the airframe through hinges. The hinges either provide or do not provide good electrical contacts between the door and the door frame. For these two different situations, one correspondingly has different penetrant electric fluxes (Q) [Ref. 2]

$$Q \simeq \begin{cases} \varepsilon_0 A\, E_{sc} & \text{when hinges do not provide good electric contact} \\ \varepsilon_0 A\, E_{sc}\, (1 + \dfrac{1}{s^2 C_s L_H})^{-1} & \text{when hinges provide good electric contact} \end{cases} \qquad (9)$$

where

$C_s \simeq 2\, \varepsilon_0\, (\ell + w)\, \Omega/\pi$

$L_H \simeq \mu_0 \pi g^2/(64\, nh)$

$\Omega \simeq 2\, \ell n\, [4\, (\ell + w)/g]$

A = area of door

ℓ, w = length and width of door

g = width of door slit

h, n = width and number of door hinges

The factor $[1 + (s^2 L_H C_s)^{-1}]^{-1}$ is of the order of 10^{-2} or lower, for a typical electrically small door. Thus, if good electric contact through the door hinges is maintained, the hinges will provide at least 40 dB attenuation to the electric penetration.

The electric penetration can be reduced further if conducting gasket is used. The conducting gasket has the effect of replacing [Ref. 2]

$$[1 + (s^2 L_H C_s)^{-1}]^{-1} \quad \text{by} \quad [1 + (s^2 L_H C_s)^{-1} + G_g/(sC_s)]^{-1}$$

in Equation 9, where

$$G_g \simeq 2\sigma_g \Lambda_g (\ell + w)/g$$

σ_g, Λ_g = effective conductivity and effective thickness of the conducting gasket

For $\sigma_g \Delta_g / g \simeq 10$ S/m, $|G_g/(sC_s)|$ is of the order of hundreds or higher. From the above discussion, it is clear that electric penetration should not be of concern for an electrically small closed door, once a good electric contact is maintained between the door and the airframe, either via hinges or conducting gasket.

The maximum magnetic flux Φ penetrating through door slits can be calculated as follows [Ref. 1]

$$\Phi \simeq \mu_o H_{sc} \frac{2\pi}{\Omega} k^{-2} \left\{ \frac{\cos (kw/2)}{\cos [k (\ell + w)/2]} - 1 \right\} \qquad (10)$$

where ℓ is the length of the side of the rectangular door which is parallel to $\vec{H}_{sc}$, and

$$k^2 = -s^2/c^2 - s\pi\mu_o\sigma_g\Lambda_g/(\Omega g) \qquad (11)$$

Equations 10 and 11 are applicable to doors with and without conducting gaskets and are derived by using the Ω-version of the asymptotic antenna theory [Ref. 7]. Because of its inherent low frequency approximation, one has to be cautious when the frequency is high and especially near resonances. A more general approach to deal with the high frequency situations is given in Section 3. The effect of the door hinges on the magnetic penetration is not as pronounced as on the electric penetration and is neglected in the equation. In fact, there is almost no effect if the hinges are on the side perpendicular to the short-circuit magnetic field.

For an electrically small door slit without conducting gasket, $k (\ell + w)/2 = \pi f (\ell + w)/c << 1$, and Equation 10 is simplified to

$$\Phi \simeq \frac{2\pi\mu_o H_{sc}}{\Omega} \frac{\ell(\ell + 2w)}{8} \qquad (12)$$

This is comparable to the penetration through a simple aperture of the same dimensions.

When conducting gasket is used so that

$$k^2 \simeq -s\pi\mu_o\sigma_g\Delta_g/(\Omega g)$$

$$|k\ell/2| > 1$$

Equation 10 can be simplified to

$$s\Phi \simeq \frac{2g}{\sigma_g\Delta_g} H_{sc} \qquad (13)$$

To monitor the electric and magnetic penetrations through a hatch aperture, such as a door slit, techniques similar to those for monitoring the penetrations through simple apertures can be employed.

3.0 MONITORING AND QUANTIFYING PENETRATION THROUGH RESONANT APERTURES

The monitoring techniques presented in Section II have the deficiency that when the frequency becomes high the response of the monitoring wire strongly depends on its detailed configuration. The resonances associated with the length of the monitoring wire might even come into play to overshadow and change the penetration behavior, such as shifting the aperture resonance frequencies. In this case, the formulas given in Section II are also not accurate, and the approximation of separating the electric and magnetic penetrations does not hold. That is to say, when the apertures are not small compared to the wavelength, one may want to resort to other monitoring techniques, and develop new formulas to estimate the corresponding responses. In this section, one of these techniques and approximate formulas will be given for hatch apertures. It is appropriate to leave out simple apertures from these more general considerations. This is because most simple apertures in aircraft are electrically small in the frequency range of 0-200 MHz.

When a door is closed or a window is equipped with hardening elements, major penetrations take place at the thin circumferential slits. As the frequency increases an efficient monitoring scheme is the one presented in Fig. 4, where a 50 Ω coaxial cable has its outer conductor grounded to the door or window frame and the inner conductor connected to the door panel or window hardening fixes (e.g., wire meshes or conductive coating). The door/window structure thus behaves as a receiving antenna with signal picked up by the coaxial cable. This slit receiving antenna with incident waves having magnetic fields parallel to the door/window frame can be modeled as the Babinet's equivalent of a loop antenna illuminated by waves having electric fields parallel to the plane of the loop. Furthermore, since most doors and windows have lengths approximately equal to their widths, the loop antenna will be modeled as circular.

The coupling to a circular loop antenna can be obtained from the equivalent circuit in Fig. 5, with the circuit elements $I^{sc}_{\ell,n}$, $Z_{\ell,n}$ and $V^{oc}_{\ell,n}$ given by [Ref. 7]

$$I^{sc}_{\ell,o} = -\frac{2aE^{i}_{o,\ell}}{\eta_o}\frac{J_1(ka\sin\theta_i)}{a_o - j2aZ'_i/\eta_o} \tag{14}$$

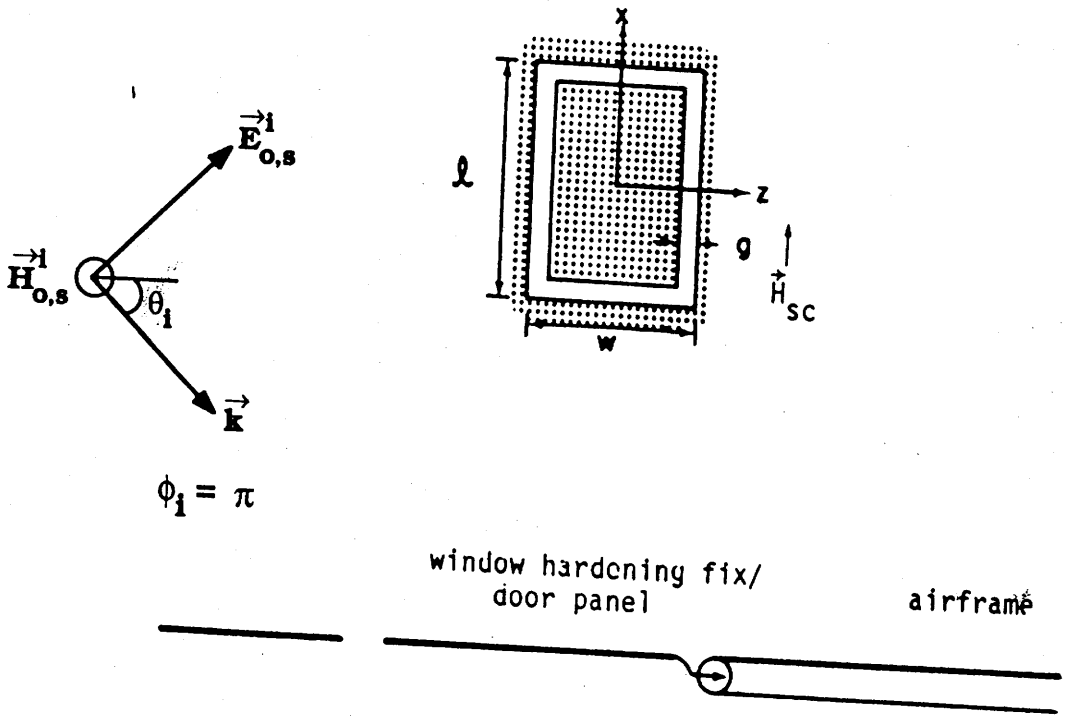

Figure 4. Scheme to monitor EMP penetrations, which is applicable for both low and high frequencies.

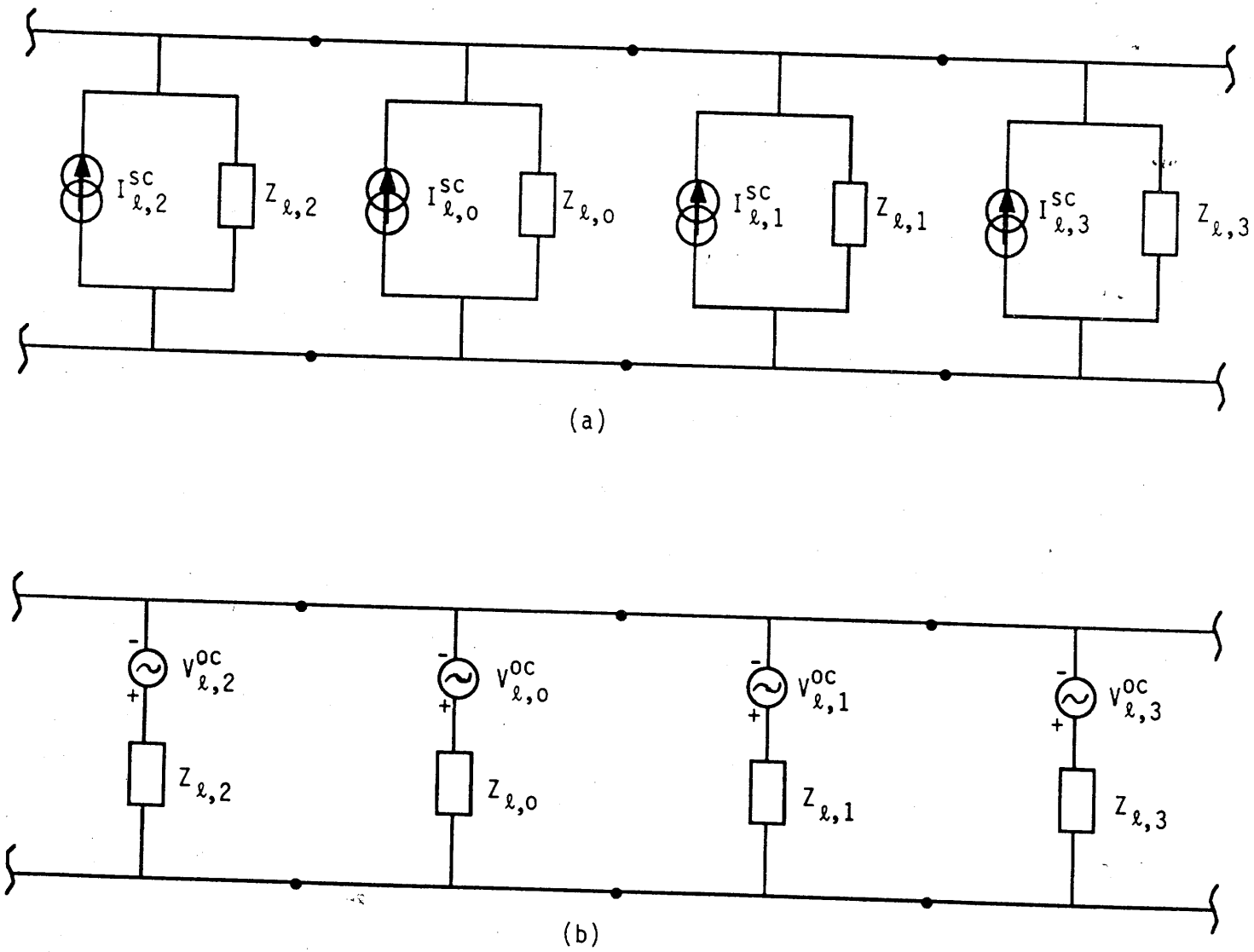

Figure 5. (a) Norton's and (b) Thevenin's equivalent circuits of a loop antenna illuminated by a plane wave with electric field parallel to the plane of the loop.

$$I^{sc}_{\ell,n} = -\frac{2aE^{i}_{o,\ell}}{n_o}\frac{[J_{n+1}(ka\sin\theta_i) - J_{n-1}(ka\sin\theta_i)]j^n\cos(n\phi_i)}{a_n - j2aZ'_i/n_o}, \quad n \neq 0$$

$$Z_{\ell,n} = jn_o\pi(2 - \delta_{no})^{-1}\,[a_n - j2aZ'_i/n_o]$$

$$V^{oc}_{\ell,n} = I^{sc}_{\ell,n}\,Z_{\ell,n}$$

where

δ_{no} = Kronecker delta function = $\begin{cases} 0, & n \neq 0 \\ 1, & n = 0 \end{cases}$

$n_o = 120\pi$, $k = \omega/c$

$J_n(\cdot)$ = Bessel's function of the first kind

Z'_1 = impedance per unit length of the equivalent loop

$= \sigma_g\Delta_g n_o^2/(4g)$

$E^{i}_{o,\ell,\theta_i,\phi_i}$ = electric field strength and incident angles of the incident wave for the loop antenna

and, a, the radius of the equivalent circular loop is approximately taken to be $(\ell + w)/\pi$ for a rectangular door/window with length ℓ and width w.

a_n is a very complicated function of frequency, a, and the slit width g. In fact, for a >> g, a_n can be approximately calculated using the following equations [Ref. 7]

$$a_n = \frac{ka}{2}(K_{n+1} + K_{n-1}) - \frac{n^2}{ka}K_n \qquad (15)$$

$$K_o \simeq \frac{1}{\pi}\ell n\left(\frac{8a}{g}\right) - \frac{1}{2}\int_o^{2ka}[\Omega_o(x) + jJ_o(x)]\,dx$$

$$K_n = K_{-n} \simeq \frac{1}{\pi}\left[K_o\left(\frac{ng}{a}\right)I_o\left(\frac{ng}{a}\right) + C_n\right] - \frac{1}{2}\int_o^{2ka}[\Omega_{2n}(x) + jJ_{2n}(x)]\,dx$$

$K_o(\cdot)$, $I_o(\cdot)$ = modified Bessel functions

$$C_n \simeq 0.57 - 2 \sum_{m=0}^{n-1} (2m+1)^{-1} + \ell n(4n)$$

$$\Omega_m(x) = \frac{1}{\pi} \int_0^{\pi} \sin(x \sin\theta - m\theta)\, d\theta$$

By applying the Babinet principle, one can then obtain, from the above loop equivalent circuit, the equivalent circuit for the coupling to the slit antenna. This slit equivalent circuit is given in Fig. 6, with circuit elements $V_{s,n}^{oc}$, $Z_{s,n}$ and $I_{s,n}^{sc}$ given by

$$V_{s,o}^{oc} = E_{o,s}^{i}\, a \frac{J_1(ka \sin\theta_i)}{a_o - ja\eta_o\sigma_g\Delta_g/(2g)} \tag{16}$$

$$V_{s,n}^{oc} = E_{o,s}^{i}\, a \frac{[J_{n+1}(ka \sin\theta_i) - J_{n-1}(ka \sin\theta_i)]j^n \cos(n\phi_i)}{a_n - ja\eta_o\sigma_g\Delta_g/(2g)}, \quad n \neq 0$$

$$Z_{s,n} = -\frac{j\eta_o}{4\pi}[a_n - ja\eta_o\sigma_g\Delta_g/(2g)]^{-1}(2 - \delta_{no})$$

$$I_{s,n}^{sc} = V_{s,n}^{oc}/Z_{s,n}$$

Since the frequency range of interest is only up to a couple of resonance frequencies, (say, $ka \lesssim 2$) the equivalent circuits can be simplified by including only a few circuit elements, say $n \leq 3$. In each frequency range where $ka \simeq n$ $(\neq 0)$, the circuit elements associated with a_n dominates, and the behaviors of $Z_{\ell,n}$ and $Z_{s,n}$ change from capacitive to inductive and from inductive to capacitive, respectively. For the circuit elements associated with a_o, $Z_{\ell,o}$ is always inductive, while $Z_{s,o}$ is capacitive. With the above understanding, the impedance elements in the equivalent circuits of Figs. 5 and 6 can be represented by resistors, inductors and capacitors as shown in Figs. 7 and 8. The exact value of these resistors, inductors and capacitors, again, are complicated function of frequency, a and g. However, they can be obtained once a_n is numerically evaluated. In the low frequency range $(ka < 0.2)$, a_n may be approximated by

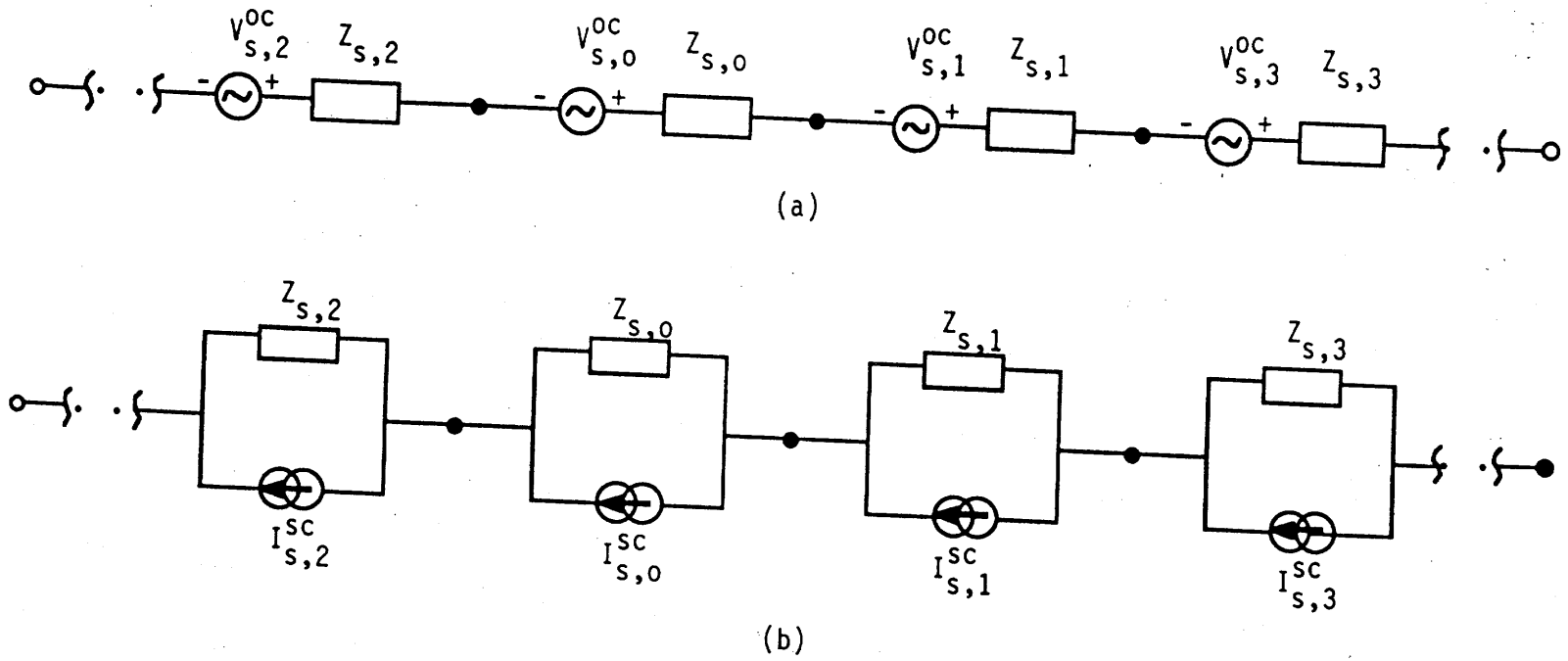

Figure 6. (a) Thevenin's and (b) Norton's equivalent circuits of a slit antenna (Babinet's complementary of a loop antenna) illuminated by a plane wave with magnetic field parallel to the plane of the slit.

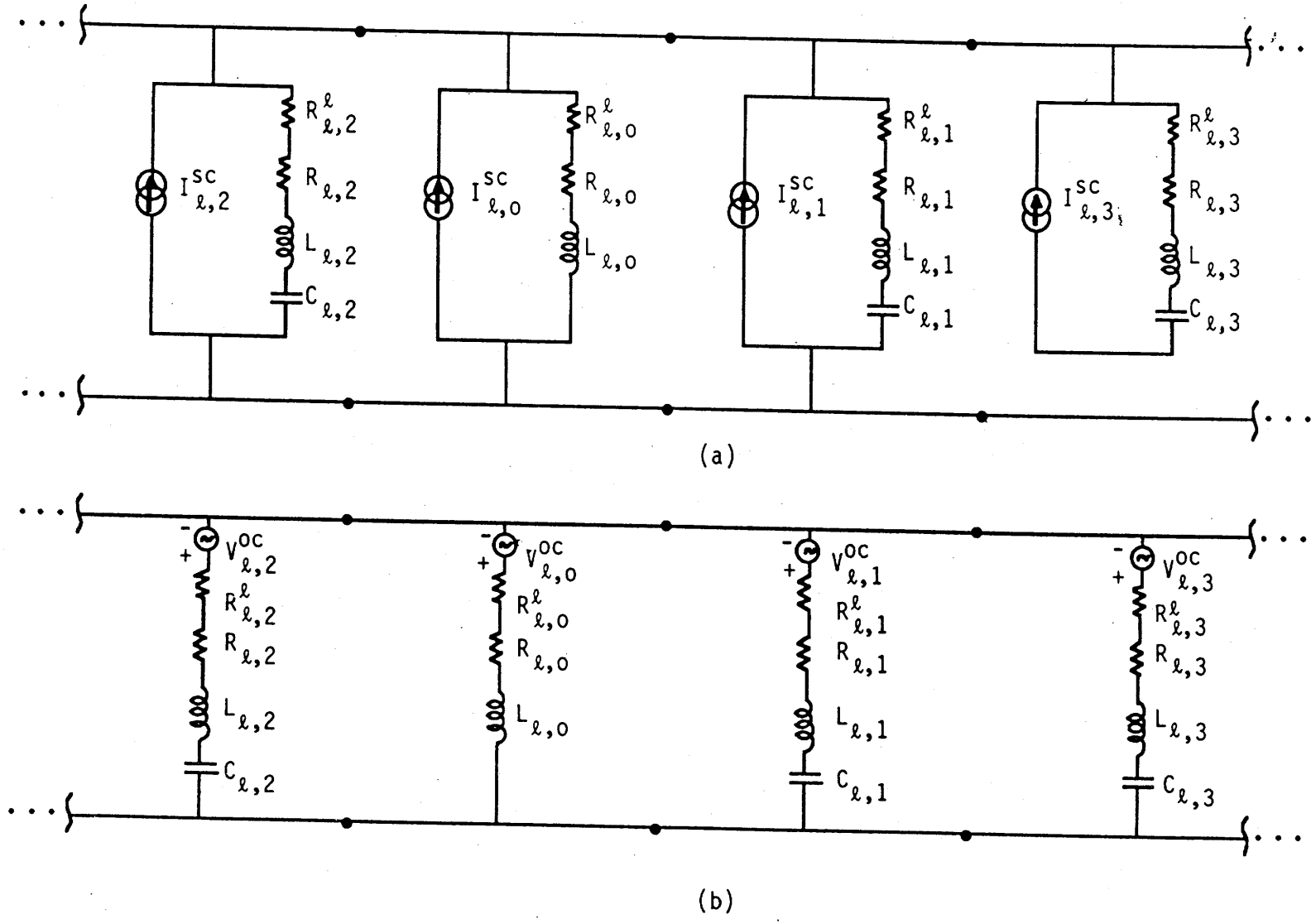

Figure 7. (a) Norton's and (b) Thevenin's equivalent circuits of a loop antenna similar to Figure 5, except that circuit elements are explicitly indicated.

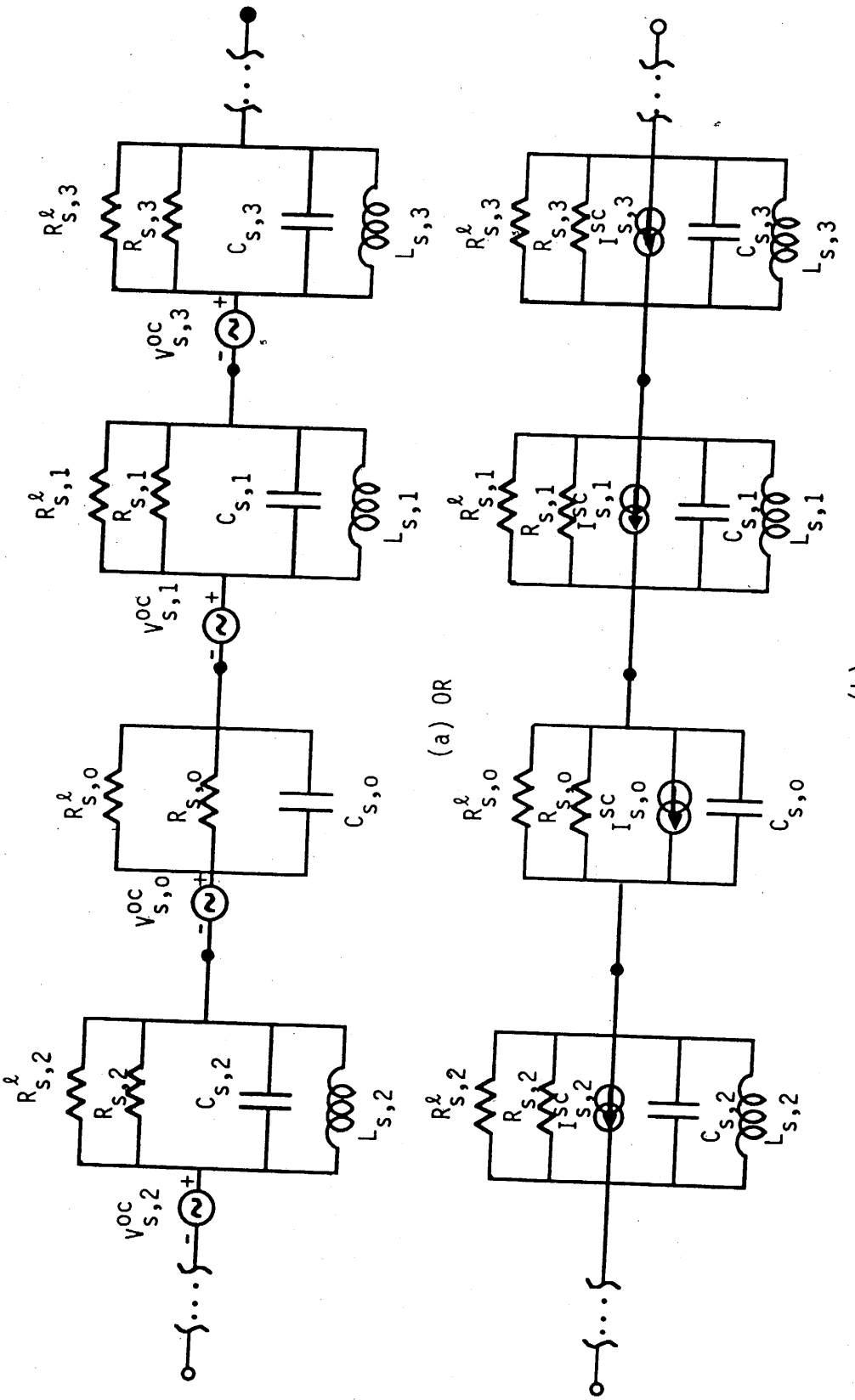

Figure 8. (a) Thevenin's and (b) Norton's equivalent circuits of a slit antenna similar to Figure 6, except that circuit elements are explicitly indicated.

$$a_o \simeq \frac{ka}{\pi} \ell n(4\pi a/g) - j(ka)^4/6$$

$$a_n \simeq -\frac{1}{\pi ka}(n^2 - k^2a^2)\, \ell n(4\pi a/g) - j\frac{(ka)^{2n}}{2\Gamma(2n)}\frac{n+1}{2n+1}, \quad n \neq 0 \tag{17}$$

With these approximations, the impedance elements in the equivalent circuits of Figs. 7 and 8 can be explicitly expressed. In Fig. 7, these impedance components for the loop antenna are:

$$L_{\ell,n} \simeq \mu_o\, a\, \ell n(4\pi a/g)/(2 - \delta_{no})$$

$$R_{\ell,o} \simeq \pi\eta_o (ka)^4/6$$

$$R^{\ell}_{\ell,n} \simeq 2\pi a\, \sigma_g \Delta_g n_o^2 (2-\delta_{no})^{-1}/(4g)$$

$$C_{\ell,n} \simeq 2\varepsilon_o a[n^2 \ell n(4\pi a/g)]^{-1}, \qquad n \neq 0 \tag{18}$$

$$R_{\ell,n} \simeq \pi\eta_o \frac{(ka)^{2n}}{4\Gamma(2n)}\frac{(n+1)}{(2n+1)}, \qquad n \neq 0$$

In Fig. 8, these impedance components for the slit antenna are

$$C_{s,n} = 4L_{\ell,n}/n_o^2 \simeq 4\varepsilon_o a\, (2 - \delta_{no})\, \ell n(4\pi a/g)$$

$$R_{s,o} = n_o^2/(4R_{\ell,o}) \simeq 3\, \eta_o (ka)^{-4}/(2\pi)$$

$$R^{\ell}_{s,n} = n_o^2/(4R^{\ell}_{\ell,n}) \simeq (2 - \delta_{no})\, (2\pi a\sigma_g \Delta_g/g)^{-1} \tag{19}$$

$$L_{s,n} = n_o^2\, C_{\ell,n}/4 \simeq \mu_o\, a\, [2n^2\, \ell n(4\pi a/g)]^{-1}, \qquad n \neq 0$$

$$R_{s,n} = n_o^2/(4R_{\ell,n}) \simeq \frac{\eta_o\, \Gamma(2n)\, (2n+1)}{\pi\, (ka)^{2n}\, (n+1)}, \qquad n \neq 0$$

It should be noted that $R_{\ell,n}$ and $R_{s,n}$ are the radiation resistances of the antennas.

The circuits given by Figs. 7 and 8, and Equations 18 and 19, evidently provide appropriate reactive and radiative behaviors near the resonance

frequencies. They also reduce to those one expects for electrically small loop antennas and door/window slits. In fact, for electrically small door/window slits (i.e., $ka \ll 1$), the circuits are dominated by the components associated with $n = 0$ and $n = 1$. The $n = 0$ and $n = 1$ components, if one ignores the radiation resistances, agree with those presented in Section 2 for electric and magnetic penetrations, respectively. At higher frequencies, if there is no conducting gasket at the slits (i.e., $R^{\ell}_{s,n} = \infty$), the presence of the radiation resistances $R_{s,n}$ will amend the deficiencies near resonance frequencies of Equation 10 in Section 2. When there are conducting gaskets, even with a moderate value of, say, $\sigma_g \Delta_g / g = 1$ S/m , $Z_{s,n} \simeq R^{\ell}_{s,n}$ for frequencies neither too high nor too low (e.g., $5 \gtrsim ka \gtrsim 0.1$). For this case, one has, for $\theta_i = \pi/2$,

$$V_s^{oc} = \sum_{n=0}^{\infty} V_{s,n}^{oc} = \frac{j\, E^i_{o,s}}{\eta_o\, \sigma_g \Delta_g / (2g)} \times$$

$$\begin{cases} [J_1(ka) - 2J_3(ka) + 2J_5(ka) - \cdots] - j[J_0(ka) - 2J_2(ka) + 2J_4(ka) - \cdots], & \phi_i = 0 \\ 0, & \phi_i = \pi/2 \\ [J_1(ka) - 2J_3(ka) + 2J_5(ka) - \cdots] + j[J_0(ka) - 2J_2(ka) + 2J_4(ka) - \cdots], & \phi_i = \pi \end{cases}$$

$$= \frac{j\, H^i_{o,s}\, 2g}{\sigma_g \Delta_g} \times \begin{cases} [\sin ka - J_1(ka)] - j \cos ka, & \phi_i = 0 \\ 0, & \phi_i = \pi/2 \\ [\sin ka - J_1(ka)] + j \cos ka, & \phi_i = \pi \end{cases} \qquad (20)$$

In Equation 20, one can take the difference between those of $\phi_i = 0$ and $\phi_i = \pi$ to obtain a result equivalent to Equation 13.

Knowing the above equivalent circuit for the door/window slits, the voltage or power picked up by the suggested monitoring coaxial cable can be obtained straightforwardly.

4.0 CHARACTERIZATION OF MONITORING DRIVER

In this section, the driving sources for the monitoring techniques suggested in the previous sections are discussed. Two kinds of drivers are proposed to excite the apertures under test: parallel-plate and two-wire simulators. In a parallel-plate simulator, as described in Fig. 9, the ratio between the height h and the half-width b of the upper plate can be properly chosen so that the characteristic impedance is 50 Ω. From Refs. 8 and 9, it is found that when the lower plate is infinitely wide, the required ratio is $h/b \simeq 0.41$. If the lower plate has a finite width, the ratio should be changed. A discussion of parallel plate drivers of finite widths is contained in Ref. 10. Once the ratio has been fixed, the choice of the actual values of the parameters is subjected to the condition of field uniformity over the tested aperture. This can generally be accomplished if the width of the upper plate is a little larger than that of the tested aperture.

A two-wire simulator above a conducting ground is also described in Fig. 9. In addition to the wire half-separation b and height h above the ground, the wire radius introduces another degree of freedom. This simulator can be driven in either the common mode (same currents flowing along the wires) or the differential mode (opposite currents flowing along the wires) by installing proper launching and terminating circuits. However, the differential mode does not provide a good field uniformity over a highly conducting airframe at the tested aperture. For this reason, only the common mode excitation will be used.

For the common mode excitation of a two-wire simulator, a high field uniformity can be achieved when $h/b \simeq \sqrt{3}$ [Ref. 11]. The issue of field uniformity has been quantified using the two-norm error over the tested aperture. Curves describing such two-norm error for different values of h/b can be found in Ref. 12.

It is very difficult to obtain a 50 Ω characteristic impedance for a common mode two-wire simulator unless very thick wires are used. However, for a simulator operated at low power, one could use transformers to bring the impedance down to 50 Ω. Table 1 lists some values of characteristic impedances as a function of the ratio h/r, r being the radius of the wire for $h/b = \sqrt{3}$.

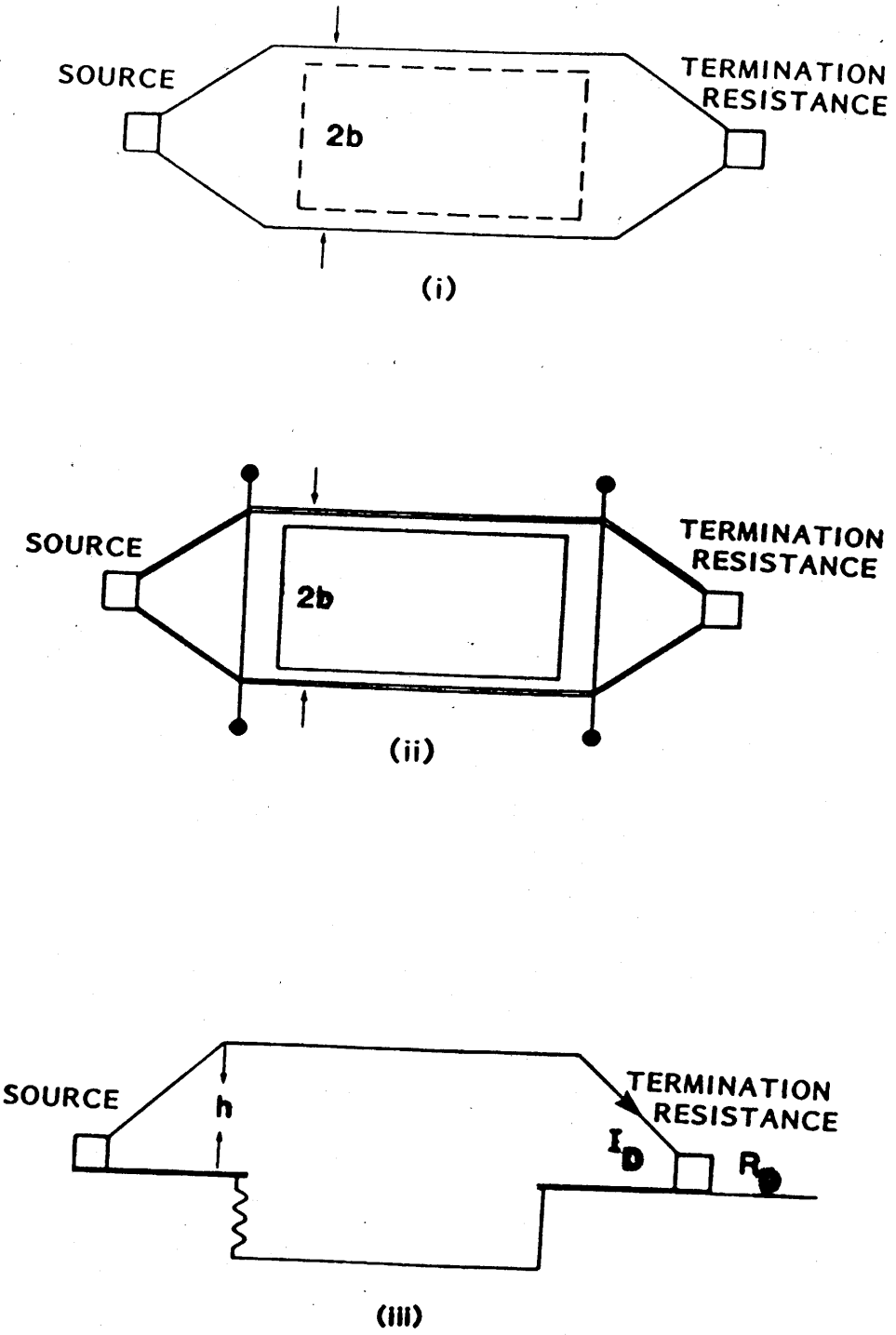

Figure 9. Schematic drawings of
(i) parallel-plate driver - top view
(ii) two-wire simulator - top view
(iii) either of above - side view

The exact field distributions of the two drivers at the tested aperture are rather complicated. In what follows, simple approximate formulas will be given.

4.1 Parallel Plate:

If the average power driving a matched transmission line (i.e., R_D, the transmission-line load, equals to Z_c) is P Watts, then

$$P = \frac{1}{2}\frac{V_o^2}{Z_c} = \frac{1}{2} I_D^2 R_D$$

where V_o is the peak voltage between the plates and I_D is the total current; that is,

$$V_o = (2 PZ_c)^{1/2} = I_D R_D \qquad (21)$$

The electric and magnetic fields at the shorted aperture can be approximated by

$$E_{sc} = \eta_o H_{sc} \simeq V_o/h = I_D R_D/h \simeq (2 PZ_c)^{1/2}/h \qquad (22)$$

If one takes $Z_c = 50\ \Omega$ and uses $h/b = 0.41$, Equation 22 becomes

$$E_{sc} = \eta_o H_{sc} \simeq 49 \sqrt{P}/(2b)\ \ (V/m)$$

where 2b can be taken to be the linear size of the tested aperture.

4.2 Two Wires:

Similarly, if the average power driving the transmission line is P watts, then

$$P = \frac{1}{2}\frac{V_o^2}{Z_c}$$

$$V_o = (2 PZ_c)^{1/2}$$

The electric and magnetic fields at the shorted aperture will be approximately given by

$$E_{sc} = \eta_o H_{sc} \simeq V_o f_E / h \qquad (23)$$

$$= \frac{(2 PZ_c)^{1/2}}{h} f_E$$

where f_E is the "electric field efficiency" defined in Ref. 11 and is given in Fig. 1 of that reference. As mentioned earlier, the desired configuration is $h/b = \sqrt{3}$. For such a configuration one has

$$E_{sc} = \eta_o H_{sc} \simeq f_{P\to E} \sqrt{P}/(2b) \ (V/m) \qquad (24)$$

$$f_{P\to E} \simeq 1.6 \sqrt{Z_c} \ f_E$$

A list of $f_{P\to E}$ for two wire simulator of various characteristic impedances is also given in Table 1.

The table indicates that the conversion factor is about 10 and E_{sc} and H_{sc} are about 1/5 of those of a parallel plate with the same P and b.

TABLE 1. CHARACTERISTIC IMPEDANCE AND FACTOR TO CONVERT POWER TO ELECTRIC FIELD FOR A TWO-WIRE SIMULATOR

h/r	CHARAC. IMPED.	$f_{P \to E}$
7	100 Ω	13
16	125 Ω	12
36	150 Ω	12
80	175 Ω	11
180	200 Ω	10
400	225 Ω	10
1000	250 Ω	9
2270	275 Ω	9
5400	300 Ω	8

5.0 COMPARISON BETWEEN QUANTIFICATION PREDICTIONS AND EXPERIMENTAL RESULTS

Measurements were performed onboard an aircraft using CW monitoring techniques presented in Section II for electrically small apertures [Ref.1]. The driver used was a 50 Ω parallel plate transmission line terminated into a matched impedance. A monitoring wire loaded with a resistance R_L was placed across either doors or windows inside the aircraft and the ratio between the voltage V_L across the load R_L and the total current on the transmission line driver I_D was obtained (see Fig. 9). This ratio is referred to as the transfer impedance of the door or window. The results of the measurements were reported in Figs. 14 and 15 of Ref. 1, which are reproduced here in Fig. 10.

5.1 Penetration Through Windows

To measure the magnetic penetration, a sensing wire loaded with R_L = 240 Ω (or 500 Ω) was placed transversally across a window, with the incident magnetic field directed along the x-axis (Fig. 4).

Equations 1, 3 and 22 give, for an electrically short sensing wire,

$$Z_T = |V_L/I_D| = \frac{\pi f \mu_o \ell^2}{2hn_o} \frac{R_L}{|j2\pi f L_m + R_L|} f_h f_g R_D \qquad (25)$$

For the window under consideration (9" x 12") the values of the parameters are

R_D = 50 Ω = parallel plate transmission line impedance

$\ell \simeq$ 30 cm

$h \simeq$ 5 cm

$L_m \simeq$ 100 nH

$L_a \simeq$ 164 nH

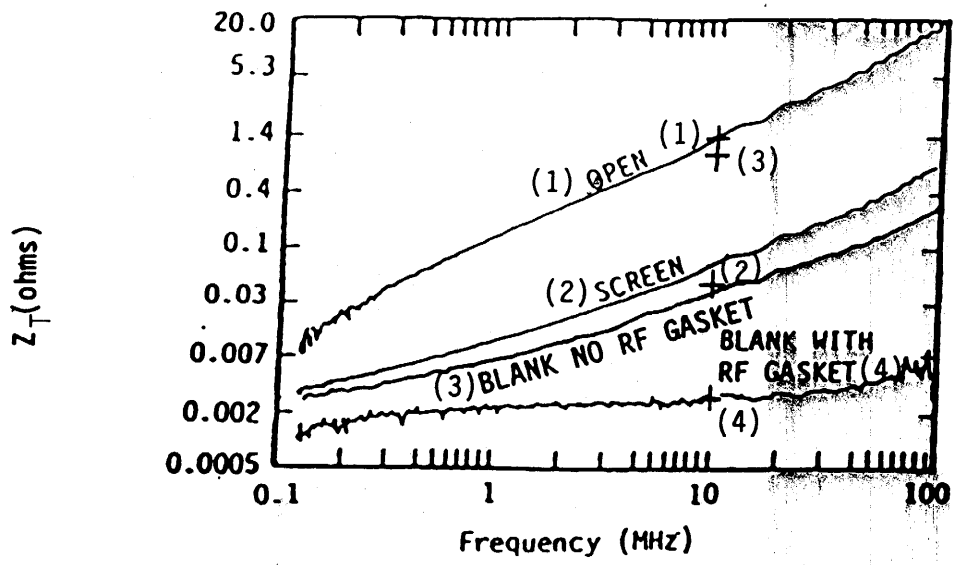

(a) measured transfer impedance of an A/C window

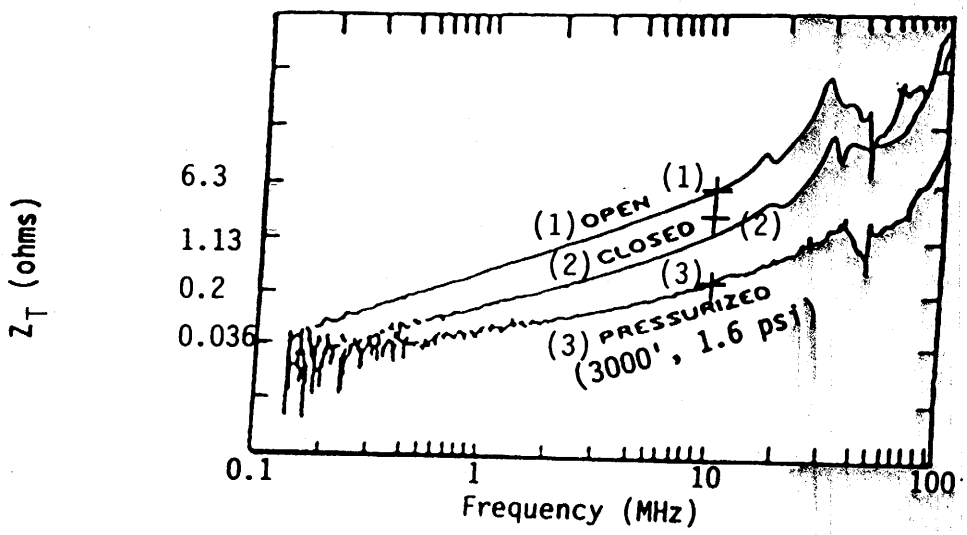

(b) measured transfer impedance of aft personnel door

Figure 10. Measured penetration for (a) window, and (b) aft personnel door of an aircraft. "+(·)" are the corresponding calculated values. The number inside (·) is used to identify window/door configurations.

$$f_h \simeq \begin{cases} 1 & \text{(unhardened window)} \\ \{1 + sL_a/[\frac{a_s}{\pi r_w^2 \sigma_w} + \frac{s\mu_o a_s}{2\pi} \ell n\ (\frac{a_s}{2\pi r_w})]\}^{-1} & \text{(wire mesh)} \\ (1 + sL_a \sigma\Delta)^{-1} & \text{(conductive coating)} \end{cases}$$

Substituting the appropriate numerical values in the above equations one obtains

$$Z_T \simeq 4.7\ f_g\ (\Omega) \qquad \text{(at 10 MHz)}$$

for the unhardened window. This value has to be compared with $Z_T = 1.4\ \Omega$ from Fig. 10a. It suggests that f_g is approximately equal to 0.3. This value of f_g will be used for a hardened window discussed below.

5.1.1 Metallic coating with conducting gasket

Assuming that the coating material has $\sigma \simeq 10^6$ S/m, and $\Delta \simeq 2$ mils one has $\sigma\Delta \cong 50$ S. Substituting in Equation 25 one finds

$$Z_T = 2.6 \times 10^{-3}\ (\Omega) \qquad \text{(at 10 MHz)}$$

which compares well with the experimental result. In addition, using 50 S for $\sigma\Delta$ in Equation 25, one observes that in the frequency range of 0.1 to 100 MHz, Z_T is almost frequency independent, in good agreement with the measured transfer impedance.

5.1.2 Metallic coating without conducting gasket

The previous result indicates that penetration through a metallic coating is small. When no conducting gaskets are used the penetration will occur mainly through a circumferential slit around the rim of the window. This penetration can be calculated using Equation 12 and assuming $\Omega = 10$ to obtain $Z_T \simeq 1\ \Omega$ at 10 MHz. This value is much higher than the measured data. This probably is because that certain electric contacts were still maintained between the coating and the window frame.

5.1.3 Wire mesh

Using $a_s = 0.1"$, $r_w = 0.002"$, $\sigma_w = 10^7$ S/m in Equ. 25, one obtains

$$Z_T = 0.04\ (\Omega) \qquad \text{(at 10 MHz)}$$

This value is a little bit lower than the measured one. This is because the calculation is performed for wire meshes in peripheral contact with the window frame, while the measurement was done for wire meshes clipped to the window frame at discrete locations. Better agreement can be obtained if this effect is included.

5.2. Penetration Through Door

Similarly to what was done for a window, a sensing wire loaded with $Z_L = 2000\ \Omega$ was placed across a door in the x direction and the transfer impedance Z_T was measured. The results for the aft personnel door are reproduced in Fig. 10b [Ref. 1]. For a closed door one can use Equations 10 and 22 to obtain

$$Z_T = |V_L/I_D| \simeq \frac{(2\pi)^2 f\, \mu_o}{\Omega h k^2 \eta_o} \left\{ \frac{\cos [kw/2]}{\cos [k(w+\ell)/2]} - 1 \right\} 50\ T f_g \qquad (26)$$

Here f_g is again introduced to account for the fact that the sensing wire does not link all the penetrant flux, and T is introduced to account for the transmission line behavior of the sensing wire when it is not short.

For the personnel door (72" x 34") the parameters assume the following values

$w \simeq 0.86$ m

$\ell \simeq 1.83$ m

$h \simeq 0.17$ m

$\Omega \simeq 15$

Substituting the parameters into Equation 25 or Equation 26, depending on whether the door is open or close, one obtains

$$Z_T = 52\ f_g T\ (\Omega) \qquad \text{(at 10 MHz)}$$

for the open door (note that at 10 MHz, $R_L = 2000\Omega >> 2\pi f L_m$, $L_m \simeq 600$ nH). From Fig. 10b it is found that $f_g \simeq 0.12$ will ensure good agreement, since at this low frequency $T \simeq 1$.

When $\lambda \simeq 2(\ell + w)$, i.e., $f \simeq 55$ MHz, the door exhibits the first resonance. Indeed from Fig. 10b one sees that there is a peak in Z_T around 55 MHz. However, this peak is overshadowed by a more pronounced peak at a lower frequency around 30 MHz. This is likely to be a resonance of the sensing wire, resulting in a large T. Since the sensing wire is placed along the x direction its length is longer than 1.83 m. Assuming its length to be a quarter wave length of a resonant dipole, the resonant frequency is then around 30 MHz. With the above discussion for an open door, the comparisons for a closed door will now follow.

When the door is hardened by conducting gaskets, one has

$$k^2 \simeq (2\pi f/c)^2 - j2\pi^2 f\mu_o\sigma_g\Delta_g/(\Omega g) \qquad (27)$$

The value of $\sigma_g\Delta_g/g$ varies with the pressure inside the aircraft. A larger value for $\sigma_g\Delta_g/g$ is expected when a higher pressure is applied. If it is assumed that $\sigma_g\Delta_g/g = 1$ S/m, the second term in Equation 27 will dominate and Z_T will be frequency independent at all frequencies in the range of 1-200 MHz. This frequency independent behavior does not appear in the measured data. This is an indication that $\sigma_g\Delta_g/g$ is smaller than 1 S/m even when the aircraft is pressurized. In fact, when it is not pressurized, $\sigma_g\Delta_g/g$ can be taken to be almost zero. Under the condition that $\sigma_g\Delta_g/g \simeq 0$ it is found that

$$Z_T \simeq 2.5\ (\Omega), \qquad \text{(at 10 MHz)}$$

which is a little bit larger than but in fair agreement with measurement data ($\simeq 2\Omega$). When the aircraft is pressurized, it appears that a value of 0.1 S/m for $\sigma_g\Delta_g/g$ can give good agreement with measurement data at 10 MHz and below. Both curves for the closed door, whether pressurized or not, show resonances around 30 MHz, at the same frequency as that of the open door. This is a further indication that the 30 MHz resonance is associated with the sensing wire rather than with the door structure. The door resonance in the open-door data (i.e., about 55 MHz) disappears in the pressurized closed door

data. This is reasonable because the conducting gasket damps out the resonance. However, all the measured data show that Z_T increases with frequency above 55 MHz, which cannot be accounted for using the simple model for electrically small apertures. It is possible that what was measured at higher frequencies had a strong contribution from electric penetration which is not included in Equations 25 and 26. From all the above considerations, it is concluded that the monitoring techniques and quantification predictions for electrically small apertures are satisfactory at low frequencies but are not satisfactory at frequencies approaching and above the resonant frequencies of the apertures. Therefore, different monitoring techniques such as those proposed in Section III may be employed at higher frequencies.

6.0 SUMMARY AND CONCLUSIONS

Techniques to monitor and quantitatively predict EMP penetration through apertures such as windows and doors of aircraft are discussed. It is first shown that when the aperture is electrically small, the penetration is decoupled into magnetic penetration and electric penetration, which can be monitored independently by using a sensing wire located across the aperture. The responses using these monitoring techniques are predicted and compared with some measurement data. The agreement is generally good when the apertures are electrically small and are not satisfactory when they are not. This is because the electric and magnetic penetrations can no longer be separated when the aperture is not electrically small. Moreover, the sensing wire may introduce spurious resonances related to its length, thus overshadowing the penetration characterization of the aperture being measured. Thus, alternative monitoring techniques need be introduced for resonant apertures. A monitoring technique which treats the aperture as a receiving antenna is then introduced for this purpose. Its expected response is also formulated. For all the suggested monitoring techniques, either a parallel-plate or a two-wire simulator can be used as the driver. Their characteristics are also given.

75 (36)

REFERENCES

1. Prather, W. D. and C. D. Taylor, "Verification of the EMP Hardening of Aircraft Windows and Doors," Hardness Surveillance Memo #2, AFWL, to be published.

2. Lee, K.S.H., editor, EMP Interaction: Principles, Techniques and Reference Data, Hemisphere Publishing Company, New York, 1986.

3. Yang, F. C. and K.S.H. Lee, "EMP Penetration Into AI Housing Through Viewing Window," etc., a series of Dikewood technical reports prepared for the Northrop Corporation, from 1982 through 1985.

4. Van Bladel, J., Electromagnetic Fields, McGraw-Hill Book Company, New York, 1964.

5. Latham, R.W., "Small Holes in Cable Shields," Interaction Notes, Note 118. AFWL, Kirtland AFB, September 1972.

6. Yang, F.C., and C.E. Baum, "Use of Matrix Norms of Interaction Supermatrix Blocks for Specifying Electromagnetic Performance of Subshields," Interaction Notes, Note 427, AFWL, Kirtland AFB, April, 1983.

7. King, R. W. P. and G. S. Smith, Antennas in Matter, The MIT Press, 1981.

8. Baum, C. E., "Impedances and Field Distributions for Parallel Plate Transmission Line Simulators," Sensor and Simulation Notes, Note 21, AFWL, Kirtland AFB, June 1966.

9. Brown, T.L., and K.D. Granzow, "A Parameter Study of Two Parallel Plate Transmission Line Simulators of EMP Sensor and Simulation Note 21," Sensor and Simulation Notes, Note 52, AFWL, Kirtland AFB, April 1968.

10. Martinez, J.P., F.C. Yang and N. Engheta, "Methodologies for Specification Verification Tests Using Shielding Enclosures," Kaman/Dikewood Report, prepared for AFWL, October 1984.

11. Baum, C. E., "Impedances and Field Distributions for Symmetrical Two Wire and Four Wire Transmission Line Simulators," Sensor and Simulation Notes, Note 27, AFWL, Kirtland AFB, June 1970.

12. Zuffada, C. and N. Engheta, "Common and Differential TEM Modes for Two Wires Above a Ground Plane," Sensor and Simulation Notes, Note 305, AFWL, Kirtland AFB, July 1987.

☆ U.S. GOVERNMENT PRINTING OFFICE: 1987—773-134/61,026